Resolution Improvement of Differential Phase-Contrast Microscopy via Tilt-Series Acquisition for Environmental Cell Application

Kazutaka Mitsuishi[1*], Fumiaki Ichihashi[2], Yoshio Takahashi[2], Katsuaki Nakazawa[1], Masaki Takeguchi[1], Ayako Hashimoto[1], and Toshiaki Tanigaki[2]

[1]National Institute for Materials Science, 1-2-1 Sengen, Tsukuba, Ibaraki, 305-0047, Japan,

[2]Research and Development Group, Hitachi, Ltd., 2520 Akanuma, Hatoyama, Saitama, 350-0395, Japan

*Correspondence should be addressed to

Kazutaka Mitsuishi, National Institute for Materials Science, 1-2-1 Sengen, Tsukuba, Ibaraki, 305-0047, Japan

Phone: +81-29-863-5474

E-mail: MITSUISHI.Kazutaka@nims.go.jp

Running title: Resolution Improvement of DPC Microscopy

Keywords: differential phase contrast, environmental cell, in situ transmission electron microscopy

Total Number of Pages: 19

Number of Figures: 5

Abstract

A simple method that improves the resolution of the phase measurement of differential phase-contrast (DPC) scanning transmission electron microscopy for closed-type environmental cell applications was developed and tested using a model sample simulating environmental cell observations. Because the top and bottom membranes of an environmental cell are typically far apart, the images from these membranes are shifted widely by tilt-series acquisition, and averaging the images after alignment can effectively eliminate undesired signals from the membranes while improving the signal from the object of interest. It was demonstrated that a phase precision of $2\pi/100$ rad is well achievable using the proposed method for the sample in an environmental cell.

Abbreviations

DPC: differential phase-contrast

Introduction

With growing environmental problems, the demand for improving the properties of functional materials is rapidly increasing. For example, catalytic nanoparticles are used for various purposes, such as CO oxidation, NO_x gas purification, selective oxidation, selective hydrogenation, and photocatalytic reactions [1], and improving their performance is strongly desired. Electron microscopy is an ideal method for analyzing these systems, and charge-state characterization correlated with catalytic activity has recently been realized using electron holography [2, 3], showing that the charge amount of nanoparticle catalysis is related to lattice distortion. To further understand the mechanism, it is important to observe these materials under actual operating conditions, such as liquid or gas atmospheres. In such *in situ* observations, closed-type environmental holders that employ electron transparent membranes to confine liquids or gases are widely used [4-8], but high-resolution observation is generally difficult because the contrasts from these membranes are superimposed on the obtained image. For example, Hyllested and Beleggia studied phase measurements using electron holography in gas environmental cell holders and reported a phase resolution of approximately 0.35 rad, stating that the degradation of phase resolution caused by the membrane is more significant than the type and pressure of gas in the environmental cell. [9] Differential phase-contrast (DPC) scanning transmission electron microscopy (STEM) [10, 11] measures electronic and/or magnetic fields by measuring the deflection of the transmitted

disk. It has been applied to a wide range of materials [12, 13], and in contrast to electron holography, it does not require a reference vacuum area, which is necessary to create an interference pattern with the electron waves that pass through the sample. This is particularly beneficial for the observation of environmental cells in which a reference area is extremely difficult—if not impossible—to obtain.

Herein, we propose a simple method that increases the phase measurement precision for an object in a closed-type *in situ* observation holder by averaging tilt-series DPC center of mass (CoM) images. Tilt-series DPC is a well-established technique that was developed to suppress diffraction contrast [14, 15] and extract electric [13] or magnetic [16] information. We used it to discriminate the information of the membranes at different heights from the region of interest.

The achievable phase measurement precision [17] is expressed as

$$\varphi_\sigma = R\sigma_{dCoM}\frac{2\pi}{\lambda}, \quad (1)$$

where R represents the spatial resolution, σ_{dCoM} represents the standard deviation of the CoM that corresponds to the precision of the detectable deflection angle, and λ represents the wavelength of incident electrons. The relationship between the electron dose and field resolution [18] is expressed as

$$\sigma_{dCoM} = \theta k_0 \begin{pmatrix} \frac{1}{2\sqrt{N_e}} \\ \frac{1}{2\sqrt{N_e}} \end{pmatrix}, \quad (2)$$

where θ represents the convergence semi-angle of the probe, k_0 represents the wavenumber, and N_e represents the number of electrons in the diffraction pattern. This is a surprisingly simple function implying that the field resolution is solely dependent on the electron dose and convergence angle and is not dependent on the camera length. This relation was derived under the assumption of statical noise, providing the theoretical lower limit of the achievable phase resolution. In the case of the observation using a cell with membranes, the phase noise due to the membrane is superimposed, and those cannot be eliminated even with infinite dose. The objective of this research is to eliminate those with tilt series acquisition. In reality, however, because DPC is a scanning technique, the position of the transmitted disk is also affected by the parallelism of the beam during the scan and how accurately the detector is electro-optically placed in the diffraction plane. Since, the previous studies only confirmed it through numerical simulation [18], we first experimentally verified the precision of the phase measurement (Eq. (2)) by measuring the standard deviation of the CoM as a function of the electron dose. The achievable phase precision was evaluated by assuming a spatial resolution R with the value expected from the convergence angle. Next, tilt-series acquisitions were applied to a model sample in which PtPd nanoparticles were deposited on a Si pillar placed between a pair of SiN membranes. Here, the field resolution was evaluated using the tilt-averaged standard deviation of the CoM of the membrane-only region, and the spatial resolution was evaluated using the Young's fringe technique with a pair of partially averaged

images [19].

Experimental

An aberration-corrected microscope (JEOL JEM-ARM200F) equipped with a high-speed pixelated STEM detector (JEOL 4DCanvas) was used at 200 kV for DPC measurement. Convergence semi-angles of 4 mrad and 22.5 μrad were used, which corresponded to the objective lens ON and OFF conditions, respectively, for measuring the relationship between dose and phase resolution. To maximize the angular resolution, each diffraction pattern was obtained with a maximum of 264 × 264 pixels, and the CoM at each scan point was calculated from these patterns. The camera lengths were adjusted such that the size of the transmitted disk (Ronchigram) was approximately 70% of the detector's field of view. Prior to data acquisition, the deflector balance for the parallel-beam scan and intermediate lens focus was carefully adjusted such that the Ronchigram did not move along with the scan. For the evaluation of the relationship between electron dose and standard deviations, the experiments were conducted in a vacuum region without any sample. For the model sample measurement, only the 4-mrad convergence semi-angle was used, because the structure was too small for a smaller convergence angle. The 4-mrad convergence semi-angle was selected considering the balance between the spatial and phase resolutions, along with the size of the model structure. The model structure, which imitated environmental cells, was fabricated on a selectively

etched Si window-supported SiN (50 nm thick) film as a lower membrane. A Si pillar was placed over it, fabricated using a focused ion beam (FIB), and the upper membrane was placed on top of the Si pillar, sliced from another area of the grid by the FIB. A schematic and transmission electron microscopy (TEM) images are shown in Figs. 1(a) and (b), respectively. To separate the films homogeneously around the pillar, a square wall was created via C deposition before placing the upper membrane. The distance between the films and the height of the edge of the Si pillar were measured via TEM by using the Fourier transform of amorphous membrane contrast (diffractogram), and the inter-membrane and pillar–membrane distances were 2.6 and 1.3 μm, respectively. The Si pillar was coated with PtPd nanoparticles that imitated catalytic particles, and these particles were used as markers for tilt-series image alignment.

[Insert Figure 1 here]

Tilt-series acquisitions were performed using originally developed acquisition software, which controls the microscope deflectors and aperture positions. It controls the aperture positions to pre-specified positions to tilt the incident direction and moves the transmitted beam to the detector position by controlling the deflector after the sample. Six sets of data were acquired consisting of 10 tilt directions with 1.6-mrad steps with the pillar placed between the membranes as the pivot point. A 264 × 264 pixel diffraction pattern was aquired for each of the 128 × 128 scan points. The tilt direction was parallel to the edge of the Si

pillar. These steps and angles were selected so that the aperture positions were well within the corrected region of the Ronchigram, which was approximately 24 mrad.

Results

Relationship between phase resolution and dose

To determine the achievable phase resolution, the relationship between the dose and the standard deviation of the CoM was evaluated. As stated previously, the phase resolution depends only on the electron dose and the convergence semi-angle of the probe. However, because the probe is scanned, the position of the transmitted disk is affected by the parallelism of the beam and a slight deviation of the detector from the back focal position. Considering the expected resolution of each convergence semi-angle, the data were acquired at magnifications of 4M and 8M for 4 mrad and 200k for 22.5 μrad, with 128 × 128 scan points. The results are summarized in Fig. 2.

[Insert Figure 2 here]

To clearly observe the effect of the scan width, the standard deviations derived from the data were separately plotted for the entire scan area, center 1/4 area, and center 1/8 area. The solid blue and orange lines in Fig. 2 correspond to the theoretical predictions (Eq. (2)). Considering that the lines indicate the theoretical lower limit of the resolution, it can be concluded that the result agrees well with the prediction. For the 4-mrad convergence semi-angle, because the

magnification is high and the phase resolution is low, the phase resolution does not strongly depend on the magnification or the scan area. Panel (b) presents a magnified image of the enclosed area in (a), which shows that it indeed depends on the scan area but is almost negligible. The green and red horizontal dotted lines represent the standard-deviation values that correspond to $2\pi/100$ rad, assuming a diffraction-limited resolution of 0.38 nm. The plot indicates that $2\pi/100$ rad can be attained using an electron dose of >1000 (e^-/pattern). For the smaller convergence semi-angle of 22.5 μm, the effect of the scan is obvious. This is due to the (two orders of magnitude) higher phase resolution, and the wider scan is due to the low magnification of 200k. A phase resolution better than $2\pi/100$ rad is still achievable using more than 1000 e^-/patterns; however, resolution improvements along the dose are hindered by the effect of the scan. When the scan area was narrowed to 1/4 and 1/8, the plot approached the theoretical limit. However, the 1/8 scan area corresponds to a magnification of 1.6 M, in which the field of view is approximately 130 nm. Because the expected spatial resolution of 22.5 μrad is approximately 68 nm, using such a high magnification is not so useful in practice. However, because the parallelism of the scan is reproducible under the same scan conditions, the effect can be compensated for using reference data obtained without a sample.

Resolution improvements via tilt-series acquisition for model sample

To improve the resolution of the environmental cell phase measurement, tilt-series acquisition was performed for the model sample, as shown in Fig. 1. According to the results discussed in the previous section, the electron currents were adjusted to approximately 4000 e^-/pattern on average in the membrane-only region; thus, each pattern in the tilt series was expected to have a base resolution better than $2\pi/100$ rad.

The membrane is amorphous in structure and is observed as a granular contrast, and since the tilt angles are still very small, the granular contrast of the films does not change much. However, because the upper and lower membranes are far from the pivot point, tilting around a Pt particle as a pivot results in a significant relative shift in opposite directions. After aligning the tilt series images with the Pt particles and superimposing them, the membrane images overlap with shifted granular contrast images, resulting in an overall reduction in contrast. On the other hand, by correcting the positions of the obtained images with pillar region and summing them, the random noise components present in each image of the tilt series are averaged and thus reduced, which improves contrast. Additionally, summing multiple images is equivalent to effectively increasing the dose. Therefore, averaging the images after aligning the position with the PtPd particles on the pillar blured the image from the membrane while improving the signal from the pillar.

Fig. 3 shows examples of the (a) first and (b) last images of a tilt series and (c) the image after averaging. Averaging was performed after aligning the tilt-series images by using the PtPd

particles on the Si pillar as position markers. The upper half of the image corresponds to the pillar region, and the lower half corresponds to vacuum (only membranes). The standard deviation in the lower region (only membranes) before averaging in (a) is 0.07 mrad. As shown in (c), after tilt-series averaging, the smoothing effect in the membrane region is evident, where the granular contrast of the membranes observed in (a) and (b) is almost completely eliminated, while the PtPd particle contrast is improved. The membrane contrasts also overlapped in the pillar region, but these contrasts moved far more upon tilting relative to the PtPd contrast on the pillar; thus, they were effectively smoothed by the averaging procedure. The standard-deviation value for the membrane region after averaging is improved to 0.03 mrad in (c).

[Insert Figure 3 here]

Spatial-resolution- evaluation of tilt-series averaged image

To evaluate the phase precision attainable via DPC, it is necessary to measure not only the standard deviation of the CoM but also the spatial resolution. Young's fringe resolution evaluation [18] was performed to evaluate the spatial resolution of the DPC images after tilt-series averaging. Regarding the photographs in the tilt-series datasets, the first half were aligned with the first image, and the remaining half were aligned with the last image, resulting in pairs of averaged images with slight shifts relative to each other. These pairs of images

were superimposed and used for the Young's fringe evaluation. Fig. 4 presents example images for the CoM of the x direction (a, b), and the CoM of the y direction (d, e). The spatial resolution was evaluated as 0.79 nm for this case. Here, the x and y directions correspond to the directions of the detector, and because they are rotated approximately 45 degrees from the direction of the sample edge on the diffraction plane, edge contrast appears in both the CoM_x and CoM_y images.

The resolution evaluation results using just two images (the first and last) were shown in Fig. 4 (c) and (f) for CoM_x, and CoM_y respectively. In comparison to the evaluations performed after aligning and summing five images shown in Fig. 4(b) and (e), the Young's fringe images created with just two images exhibit poorer contrast. Specifically, there is a slight degradation in the x direction and a more pronounced degradation in the y direction. This indicates that, due to the small tilt angle increment of 1.6 mrad and a total tilt of only 16 mrad which is well within the aberration corrected phase flat area of around 15 mrad (semi-angle), the changes of the aberrations between individual images are minimal when acquiring the tilt series. Consequently, the improvement in the signal-to-noise ratio from summing the images leads to an overall enhancement in resolution, outweighing any degradation in resolution from overlaying different images.

[Insert Figure 4 here]

The evaluated spatial resolutions for all the datasets are presented in Fig. 5, together with the

standard deviation of the CoM of the vacuum (membranes only) regions (lower part of the tilt-series averaged image). As indicated by Eq. (1), the achievable phase resolution can be determined using a pair of spatial resolutions and the standard deviations of the CoM. The dotted line indicates the boundary below which the resolution of $2\pi/100$ rad is achieved. As shown, most of the datasets are well within the range, suggesting that the phase resolution of $2\pi/100$ rad can be achieved using the proposed tilt-series acquisition method by minimizing the film contrast for the sample in an environmental cell.

[Insert Figure 5 here]

Discussion

Here, we discuss the comparison between the proposed method and the method of using a large convergence angle to improve depth resolution. Assuming the angle range typically correctable by an aberration corrector is 30 mrad, the depth obtained as the FWHM (Full Width at Half Maximum) of the probe intensity is $\Delta z = 1.77\ \lambda/\alpha^2$, which is approximately 5 nm, providing sufficient resolution to clearly resolve the center of the environmental cell. Furthermore, with a convergence angle of 30 mrad, the probe spread at the position of the membrane, which is 1.3 μm away from the focal point, is $1.3\ \mu$m × 0.03 rad = 39 nm in radius, or 78 nm in diameter. This means that the influence of the amorphous structure within this range will be averaged out, thus significantly reducing the membrane contrast. However,

increasing the convergence angle in DPC reduces the resolution of the detected deflection angle changes. As shown by Equation (2), when the dose is kept constant, the standard deviation increases proportionally with the convergence angle making it difficult to detect small deflection angles, such as those caused by the potential distributions around catalyst nanoparticles. Therefore, it is necessary to choose an appropriate convergence angle according to the target to be measured. On the contrary, reducing the influence of the membrane by acquiring a tilt series can be done independently of the choice of convergence angle, allowing the convergence angle to be freely chosen according to the target of observation.

Conclusion

A simple technique to improve the resolution of the phase measurement of DPC for environmental cell applications was developed and tested using a model sample simulating environmental cell observations. The relationship between the dose and the attainable CoM precision was tested for two convergent semi-angles that coincided well with theoretical predictions. The pairs of spatial resolutions and standard deviation of the CoM were evaluated for the images obtained via tilt-series acquisition, and the results indicated that $2\pi/100$ rad is well achievable using the proposed tilt-series acquisition method for the sample in an environmental cell.

Funding

This work was supported by the Innovative Science and Technology Initiative for Security, Acquisition, Technology, and Logistics Agency, Japan [grant number JPJ004596].

Conflict of interest

The authors declare that they have no conflict of interest.

Acknowledgement

We would like to thank Editage (www.editage.jp) for English language editing.

References

1. Liu, L. and A. Corma, *Metal Catalysts for Heterogeneous Catalysis: From Single Atoms to Nanoclusters and Nanoparticles.* Chem Rev, 2018. **118**(10): p. 4981-5079.
2. Aso, R., et al., *Direct identification of the charge state in a single platinum nanoparticle on titanium oxide.* Science, 2022. **378**(6616): p. 202-206.
3. Aso, R., et al., *High-precision charge analysis in a catalytic nanoparticle by electron holography.* Microscopy (Oxf), 2024.
4. Williamson, M.J., et al., *Dynamic microscopy of nanoscale cluster growth at the solid-liquid interface.* Nat Mater, 2003. **2**(8): p. 532-6.
5. Ring, E.A. and N. de Jonge, *Microfluidic system for transmission electron microscopy.* Microsc Microanal, 2010. **16**(5): p. 622-9.
6. Ye, F., et al., *In Situ TEM Studies of Catalysts Using Windowed Gas Cells.* Catalysts, 2020. **10**(7).
7. Qu, J., M. Sui, and R. Li, *Recent advances in in-situ transmission electron microscopy techniques for heterogeneous catalysis.* iScience, 2023. **26**(7): p. 107072.
8. Yaguchi, T., et al., *In-situ TEM study from the perspective of holders.* Microscopy (Oxf), 2024. **73**(2): p. 117-132.
9. Hyllested, J.A.E. and M. Beleggia, *Investigation of gas-electron interactions with electron holography.* Ultramicroscopy, 2021. **221**: p. 113178.
10. Shibata, N., et al., *Direct Visualization of Local Electromagnetic Field Structures by Scanning Transmission Electron Microscopy.* Acc Chem Res, 2017. **50**(7): p. 1502-1512.
11. Shibata, N., et al., *Differential phase-contrast microscopy at atomic resolution.* Nature Physics, 2012. **8**(8): p. 611-615.
12. Kohno, Y., et al., *Real-space visualization of intrinsic magnetic fields of an antiferromagnet.* Nature, 2022. **602**(7896): p. 234-239.
13. Toyama, S., et al., *Real-space observation of a two-dimensional electron gas at semiconductor heterointerfaces.* Nat Nanotech, 2023. **18**(5): p. 521-528.
14. Nakamura, A., et al., *Differential Phase Contrast Imaging with Reduced Dynamical Diffraction Effect.* Microscopy and Microanalysis, 2017. **23**(S1): p. 1412-1413.
15. Kohno, Y., et al., *Development of tilt-scan system for differential phase contrast scanning transmission electron microscopy.* Microscopy (Oxf), 2022. **71**(2): p. 111-116.
16. Murakami, Y.O., et al., *Magnetic-structure imaging in polycrystalline materials by specimen-tilt series averaged DPC STEM.* Microscopy (Oxf), 2020. **69**(5): p. 312-320.
17. Ishikawa, R., et al., *Spatial and phase resolution in electron microscopy.* Microscopy (Oxf), 2023. **72**(2): p. 78-96.

18. Pollath, S., F. Schwarzhuber, and J. Zweck, *The differential phase contrast uncertainty relation: Connection between electron dose and field resolution.* Ultramicroscopy, 2021. **228**: p. 113342.
19. Weiss, F.Z.K., *Young's interference fringes in electron microscopy revisited.* Ultramicroscopy, 1993. **50**(50): p. 123.

Figure Legends

Fig. 1 (a) Schematic of the model sample structure and tilt-series acquisition; (b) TEM image of a model sample.

Fig. 2 (a) Relationship between the electron dose and the standard deviation of the CoM for convergence semi-angles of 4 mrad and 22.5 μrad. (b) Magnified image of the enclosed region in (a). The solid lines represent theoretical predictions, and the dotted lines represent standard deviations that correspond to the phase precision of $2\pi/100$ rad, assuming diffraction-limited spatial resolutions.

Fig. 3 Example images of tilt-series acquisition of the Si pillar edge region of the model sample. The upper half of the image corresponds to the pillar region, and the lower half of the image corresponds to the vacuum (only membranes). (a) First and (b) last images of a tilt-series and (c) the image after averaging. The averaging was performed after aligning tilt-series images by using PtPd particles on the Si pillar as position markers.

Fig. 4 Example images for Young's fringe spatial resolution evaluation of tilt-series acquisition of the Si pillar edge region of the model sample. Regarding the photographs in tilt-series datasets, the first half were aligned with the first image, and the remaining half were aligned with the last image. The resultant pair of images were superimposed and used for

Young’s fringe evaluation. (a) Resultant averaged image of CoM_x; (b) Fourier transform of (a); (d) CoM_y; (f) Fourier transform of (d). (c) and (f) are the Young’s fringe evaluation result using just two images (the first and last) for CoM_x, and CoM_y, respectively.

Fig. 5 Plot of the spatial resolution versus the standard deviation of the CoM, showing the achievable phase resolution. The dotted line indicates the boundary below which the resolution of $2\pi/100$ rad is achieved.

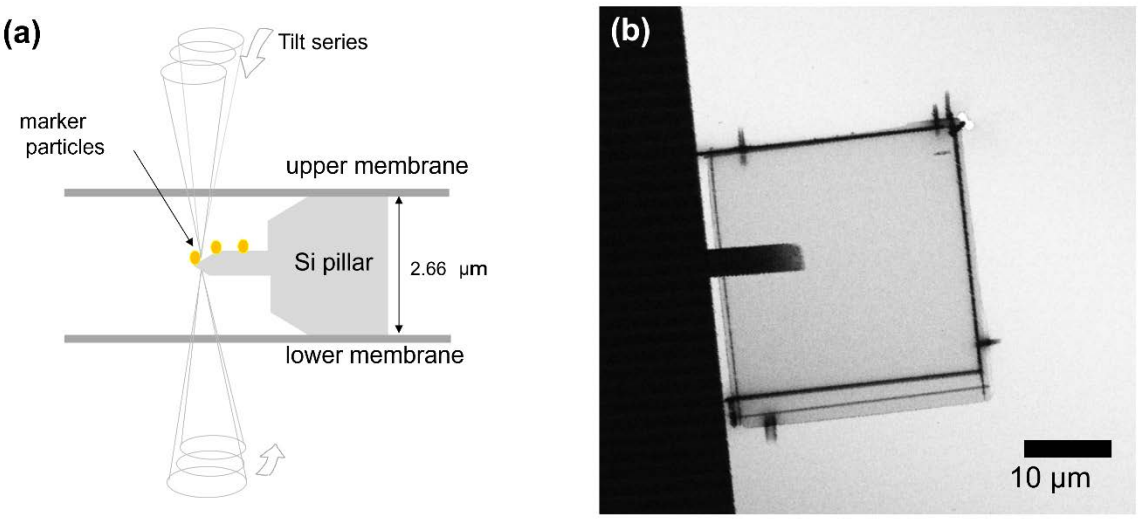
(a)
Tilt series
marker
particles
upper membrane
Si pillar
2.66 µm
lower membrane
(b)
10 µm

Figure 1

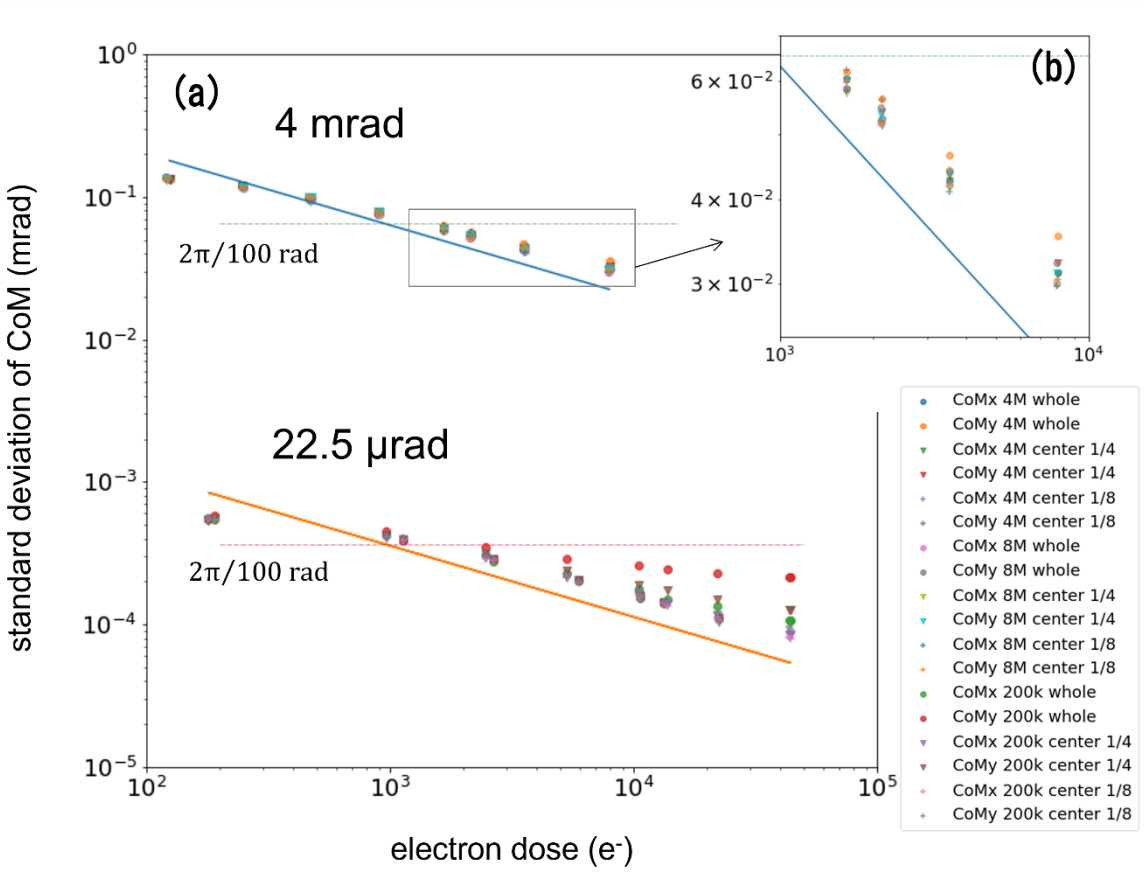

337

338 Figure 2

339

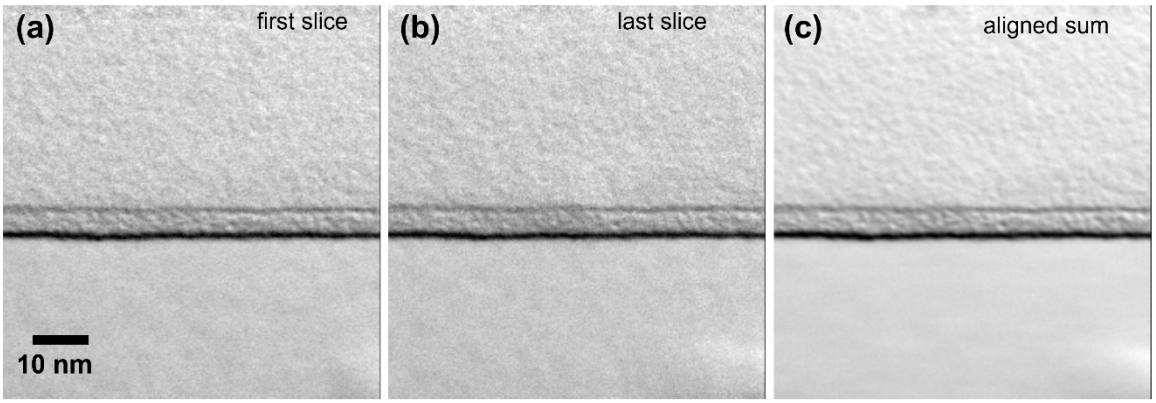

340

341 Figure 3

342

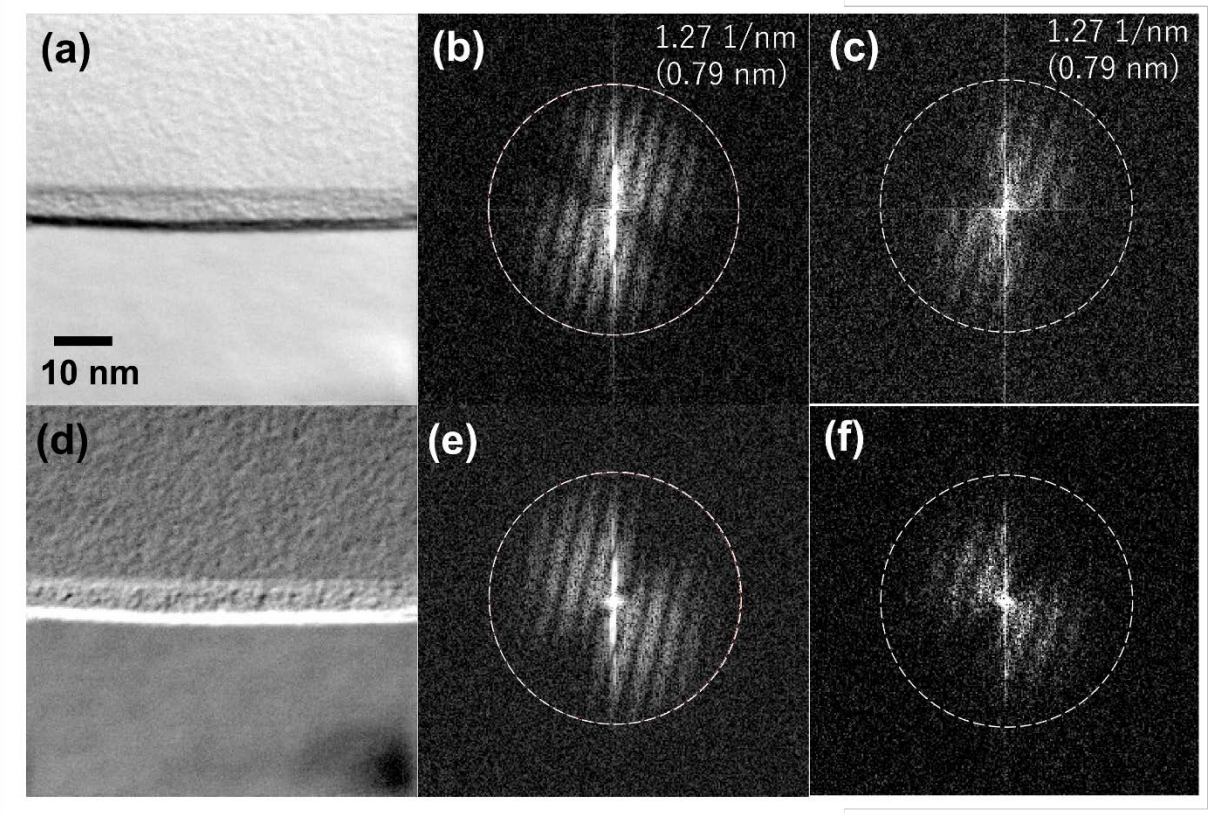

Figure 4

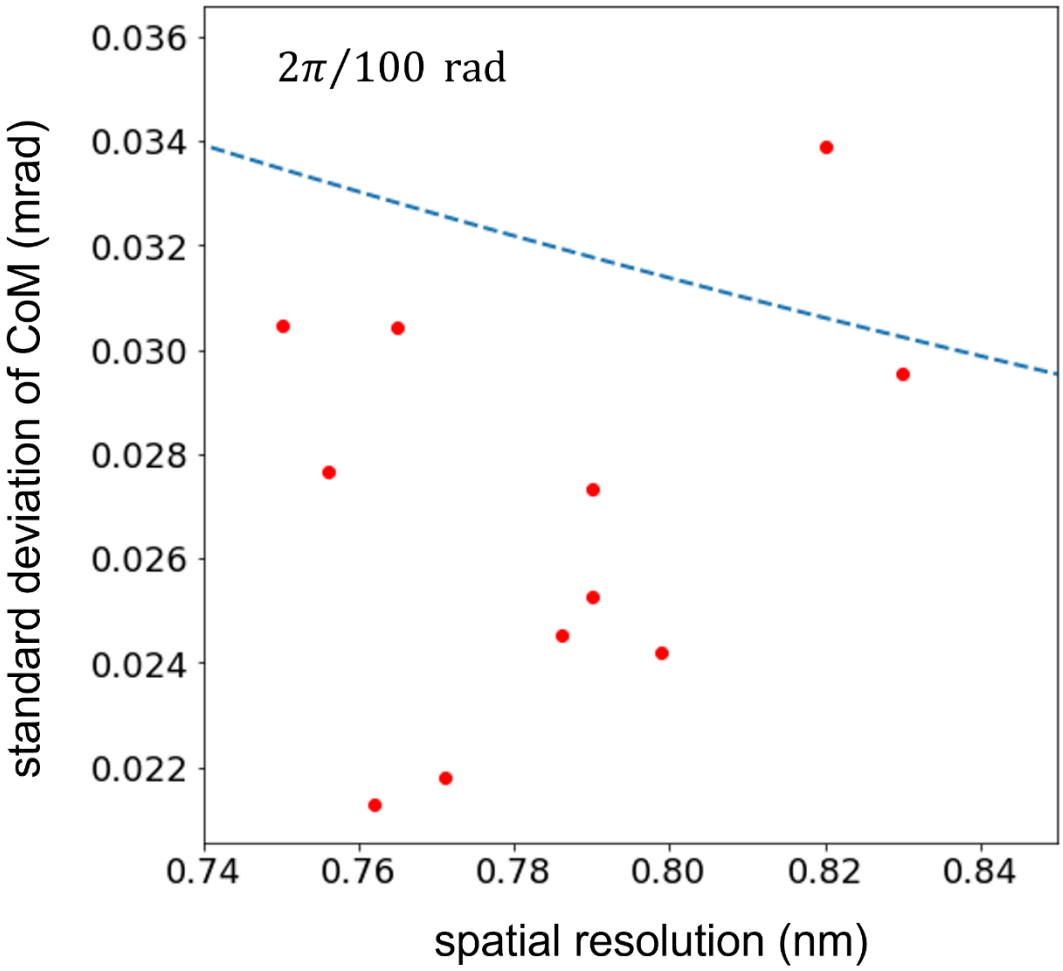

346

347 Figure 5